Density Functional Study of Electronic, Magnetic and Hyperfine Properties of $[M(CN)_5NO]^{2-}$ (M=Fe, Ru) and Reduction Products

J. A. Gómez and Diana Guenzburger

Centro Brasileiro de Pesquisas Físicas - CBPF

Rua Xavier Sigaud 150

CEP: 22290-180 Rio de Janeiro, RJ, Brasil

ABSTRACT

The Discrete Variational method (DVM) in Density Functional theory was employed to investigate the electronic structure of the complexes $[Fe(CN)_5NO]^{2-}$ (Nitroprusside), $[Fe(CN)_5NO]^{3-}$, $[Fe(CN)_4NO]^{2-}$, $[Ru(CN)_5NO]^{2-}$ and $[Ru(CN)_5NO]^{3-}$. Total energy calculations revealed that in pentacyanonitrosylferrate(I) and pentacyanonitrosylruthenate(I), which are paramagnetic ions containing one unpaired electron, the M–N–O angle is bent, having values of 152.5^o and 144^o , respectively. From self-consistent spin-polarized calculations, the distribution of the unpaired electron in the paramagnetic complexes $[Fe(CN)_5NO]^{3-}$, $[Fe(CN)_4NO]^{2-}$ and $[Ru(CN)_5NO]^{3-}$ was obtained, as well as spin-density maps. A long-standing controversy regarding the configuration of $[Fe(CN)_5NO]^{3-}$ was elucidated, and it was found that the unpaired electron in this complex is in an orbital primarily localized on π^* (NO). Mössbauer quadrupole splittings on Fe and Ru were derived from calculations of the electric-field gradients. Magnetic hyperfine coupling constants on N of the NO ligand were also obtained for the paramagnetic complexes.

I. Introduction

The chemistry of covalent transition-metal coordination compounds containing the ligand NO has been for a long time the subject of great interest. In particlar, the ion pentacyanonitrosylferrate(II) (Nitroprusside), $[Fe(CN)_5NO]^{2-}$, has been investigated extensively since the ‘60s and ‘70s . Experimental studies include electronic spectra [1], X-ray crystallography [2],[3], Mössbauer spectroscopy [4]-[6], infra-red spectroscopy [7], neutron diffraction [8] and X-ray photoelectron spectra [9]. Electronic structure studies were performed with a semi-empirical method [1], and, more recently, with an approach based on Density Functional Theory (DFT) [10]. The bonding of the transition element to the ligand NO (nitric oxide) is quite unique, since NO has an outstanding capability of forming a strong bond with Fe, in which it receives electrons into a π^* orbital through the mechanism of back-donation. The isoelectronic complex $[Ru(CN)_5NO]^{2-}$ has also been investigated by optical spectroscopy [11], X-ray crystallography [12] and Mössbauer spectroscopy [13]; Molecular Orbital calculations were performed with the Extended Hückel method [11]. Finally, the crystal structure and spectroscopic properties of $[Os(CN)_5NO]^{2-}$ were recently reported [14].

The research on Nitroprusside has undergone a revival in recent years, due mainly to two reasons. One motivation is the increasing relevance found for the NO molecule in biological processes [15]. Nitroprusside has long been known to be a potent hypotensive agent; its therapeutic properties depend on the release of nitric oxide in the appropriate biological setting. Furthermore, NO has been also found to play an important role as a messenger between neurons at synapses in the central nervous system, and to be produced by macrophages to kill invasive cells.

Another source of recent interest is the existence of long-lived metastable excited states of nitroprusside [3], [16],[17]. The first of these states characterized may be created by irradiation of the crystal with laser blue-green light of wavelength 400-530nm below 190K, and may be erased by laser irradiation with red light of 600-800nm . This property has been proposed as the basis of an information storage system, since information may be written and erased without distruction of the complex . Interesting optical properties such as holographic gratings may be obtained in $Na_2[Fe(CN)_5NO]$ and $Ba[Fe(CN)_5NO]$, due to the existance of the extremely long-living metastable states [18].

On the other hand, the nature of the products obtained by electrochemical reduction of Nitroprusside or chemical reduction with $[BH_4]^-$, ascorbic acid and other acid agents, has been the subject of considerable controversy over the years. In solution, a blue species and a brown species are formed. The blue species has been simultaneously characterized by UV and EPR spectra as

$[Fe(CN)_5NO]^{3-}$ with the outer unpaired electron in an orbital of mainly Fe $3d_z^2$ composition [19], as the protonated complex $[Fe(CN)_5NOH]^{2-}$ [20],[6] and as the tetracyano complex $[Fe(CN)_4NO]^{2-}$ formed by loss of the ligand CN trans to the NO [21]. The brown species has been identified concomitantly with $[Fe(CN)_5NO]^{3-}$ with the unpaired electron in an orbital mainly on the π^* of NO [20],[21] and with $[Fe(CN)_5NO_2]^{5-}$ [22]. Reduction products detected by ESR spectroscopy were obtained also by single crystal irradiation with γ-rays [23] or 2-MeV electrons [24], and by ultraviolet photolysis at 77K [25].

The long-standing controversy about the reduction products of Nitroprusside may only be clarified by electronic structure calculations with a non-empirical method. We report the results of calculations with the Discrete Variational method (DVM) [26],[27] in the frame of Density Functional theory (DFT) [28] for the low-spin diamagnetic complexes $[Fe(CN)_5NO]^{2-}$ (Nitroprusside) and $[Ru(CN)_5NO]^{2-}$, and for the reduced paramagnetic species $[Fe(CN)_5NO]^{3-}$, $[Fe(CN)_4NO]^{2-}$ and $[Ru(CN)_5NO]^{3-}$. The calculations are spin-polarized in the case of the paramagnetic ions. The molecular orbitals are expanded as linear combinations of numerical atomic orbitals, and the set of Kohn-Sham equations solved self-consistently in a three-dimensional grid of points. The basis of atomic orbitals allows the interpretation of the results through a Mulliken population analysis, which gives the distribution of the electrons among the orbitals of the atoms in the complexes, thus providing an understanding of the electronic phenomena in terms of a simple comprehensive picture. In addition, spin magnetic moments on the atoms may be obtained, defined as the difference between spin up (+1/2) and spin down (–1/2) populations. This analysis is not possible with the DFT methods that utilize Gaussian basis sets. In addition to the electronic structure, we also calculated quadrupole splittings (ΔEQ) at the transition element site and hyperfine coupling constants at the N of NO. The results obtained, together with reported experimental values of the properties, form a coherent picture that elucidates many aspects of the nature of the reduction products of $[Fe(CN)_5NO]^{2-}$. In the case of the Ru complexes, some predictions are made, to be tested by future measurements.

In section II we describe briefly the DV method as employed here; in section III we present results for the electronic structure, in section IV the hyperfine parameters are given and the results discussed . In section V we summarize our main conclusions.

II Theoretical Method

The DV method has been described extensively in the literature [26],[27], here we give a summary of its main features and details pertaining to the present calculations. One seeks the solution of the set of one-electron Kohn-Sham equations [28] (in Hartree atomic units):

$$[-\nabla^2/2 - \sum_q Z_q / |\mathbf{r} - \mathbf{R_q}| + \int \rho(\mathbf{r'}) / |\mathbf{r} - \mathbf{r'}| d\mathbf{r'} + V_{xc}^{\sigma}] \phi_{i\sigma}(\mathbf{r}) = e_{i\sigma} \phi_{i\sigma}(\mathbf{r}) \quad (1)$$

where V_{xc}^{σ} is the exchange-correlation potential, for which we employed the functional of Vosko, Wilks and Nusair (VWN) [29], and the electron density $\rho_{i\sigma}$ for each spin σ is given by:

$$\rho_{i\sigma}(\mathbf{r}) = \sum_i n_{i\sigma} |\phi_{i\sigma}(\mathbf{r})|^2 \quad (2)$$

where $n_{i\sigma}$ is the occupation of molecular spin-orbital $\phi_{i\sigma}$. The spin density at point **r** is defined as $[\rho\uparrow(\mathbf{r}) - \rho\downarrow(\mathbf{r})]$, where up and down arrows represent electrons of $m_s = +1/2$ and $-1/2$, respectively. In the present spin-polarized calculations, $\rho\uparrow$ has the freedom to be different from $\rho\downarrow$, as driven by the exchange interaction. The molecular spin-orbitals are expanded on a basis of numerical atomic orbitals χ_j, obtained by DFT calculations for free atoms:

$$\phi_{\sigma i}(\mathbf{r}) = \sum_j \chi_j(\mathbf{r}) c_{i\sigma}^{j} \quad (3)$$

Minimizing an error function as defined in the DV method, one obtains the secular equations formally identical to those of the Rayleigh-Ritz variational method:

$$([H] - [E][S])[C] = 0 \quad (4)$$

where [H] is the Kohn-Sham Hamiltonian matrix, [S] the overlap matrix and [C] the matrix of the coefficients in expansion (3). These equations are solved self-consistently, on a three-dimensional grid of points. The self-consistent criterium for the present calculations was $<10^{-5}$ in the density. The numerical grid is pseudorandom (diophantine) [26] in all the molecular space except inside spheres centered at the nuclei of the atoms and containing the core electrons, where the point distribution is systematic and the necessary integrations are performed precisely [30]. For the

present calculations, a very large total number of points was necessary for the self-consistent step (~230,000), due in part to the sparce distribution of the atoms in the volume of the complexes, as well as the sensitive properties calculated, such as the hyperfine parameters. For determination of the total energies, a somewhat larger number of points was employed (~280,000).

A Mulliken-type population analysis is performed [31], in which the atomic orbital occupancy is obtained from the coefficients of the LCAO expansion and the overlap populations, which are divided proportionally to the atomic coefficients in the bonds. This procedure avoids the spurious negative populations, common for transition-metal complexes when the original Mulliken populations are employed. Mulliken populations allow the analysis of the charge distribution in the complexes, and are also used in the definition of magnetic moments μ of the atoms ($\mu = 2\mu_B S$, where μ_B is the Bohr magneton), as the difference between spin up and spin down total populations. After a cycle of iterations, optimization of the numerical atomic basis was performed by utilizing the atomic configurations, obtained for the complex by the Mulliken analysis, in new atomic calculations, to obtain basis functions more adequate to the molecular environment. This procedure is repeated until the configurations obtained are approximately the same as in the basis. For Fe, the valence basis includes 3s, 3p, 3d, 4s and 4p, for Ru 4s, 4p, 4d, 5s and 5p; for C, N and O, 2s and 2p. The valence orbitals are explicitly orthogonalized to the core in the first iteration.

To render tractable the Coulomb electron-electron interaction, a model potential is considered, defined by a multicenter multipolar expansion of the density, which is fitted in each iteration to the “real” density by a least-squares fitting procedure [32]. In the present calculations all terms in the expansion up to $l = 1$ were considered. For the complexes $[Fe(CN)_5NO]^{3-}$ and $[Ru(CN)_5NO]^{3-}$, total energy calculations [33], [27] were performed for different M–NO distances and M–N–O angles (M ≡ Fe, Ru), to obtain the equilibrium values. Non-local corrections to the exchange-correlation interaction were included in this step, according to Becke [34] for exchange and Perdew [35] for correlation.

III. Electronic Structure

For the diamagnetic complexes $[Fe(CN)_5NO]^{2-}$ and $[Ru(CN)_5NO]^{2-}$, the atomic coordinates have been determined by X-ray diffraction (refs. [2] and [12], respectively). The structure of tetracyanonitrosylferrate(I) has also been determined experimentally [21a]. Therefore, for these complexes the measured values of the coordinates were used in the calculations. To our knowledge,

no determination of the structure of the paramagnetic complexes $[Fe(CN)_5NO]^{3-}$ and $[Ru(CN)_5NO]^{3-}$ has been reported so far. Preliminary calculations utilizing the same coordinates as in the diamagnetic complexes have shown that the outer unpaired electron occupies an orbital almost entirely localized on the Fe-N-O (or Ru-N-O) group of atoms. Therefore, rather than optimizing the structural parameters of the complete complexes (which was not the scope of the present study), only the M-N distance and M-N-O angle were varied, and the values of the M-N equilibrium distance and M-N-O equilibrium angle optimized by performing total energy calculations. All other structural parameters of the reduced complexes were kept the same as in the corresponding diamagnetic cases, since any possible variation from these values may be considered very small, and thus would not affect the present results in any significant manner. Test calculations to determine the same parameters in the diamagnetic complex $[Fe(CN)_5NO]^{2-}$ gave values which are accurate to within 3-4%.

In Table I are given the values of the M-N distances and M-N-O angles for the non-magnetic and the paramagnetic complexes $[M(CN)_5NO]^{n-}$. In Fig. 1a is given a representation of $[Fe(CN)_5NO]^{3-}$, showing the M-N-O angle θ. A similar figure would represent $[Ru(CN)_5NO]^{3-}$. Since in the diamagnetic complexes the axial group of atoms ON–M–CN are almost collinear, they have approximately C_{4v} symmetry, but in fact small distortions of the distances and angles remove all symmetry elements. Accordingly, no symmetry was imposed in the calculations for any of the complexes. X-ray diffraction of the tetracyano complex also revealed an approximately colinear Fe–NO group, with d (Fe-N0) = $1.565A^0$ and θ = 177.1° (see Fig. 1b).

In Table I, we see that the M-N distance is increased in the reduced complexes with respect to the values in the corresponding diamagnetic complexes, as would be expected from intuitive considerations, since the added electron increases the electron-electron repulsion in the bond. The angle θ is considerably reduced in the paramagnetic complexes, as compared to θ in the corresponding diamagnetic complexes. Figs. 2 and 3 show the variation of the total energy of $[Fe(CN)_5NO]^{3-}$ and $[Ru(CN)_5NO]^{3-}$, respectively, with the M-N distance (2a and 3a) and with the M-N-O angle θ (2b and 3b). Apart from the equilibrium value, other more shallow minima are noticed in the dependence of the energy with θ. The bending of the Fe-N-O bond in $[Fe(CN)_5NO]^{3-}$ has been predicted qualitatively on the basis of analysis of the molecular orbitals [36], [37], and by combining results of EPR measurements with molecular orbitals considerations [20].

In Table II are given the atomic charges, Mulliken populations and spin magnetic moments of $[Fe(CN)_5NO]^{2-}$, $[Fe(CN)_5NO]^{3-}$ and $[Fe(CN)_4NO]^{2-}$. In the diamagnetic complex the charge on

Fe is approximately +1 (far from the formal value +2) with the main contributions on the Fe coming from 3d and 4p. The C atoms on the CN ligands have rather small positive charges with large negative charges on the N of the CN. The N of the NO ligand has a small positive charge and the O a charge of ~ –0.2. Approximately the same charge distribution is observed in the derived paramagnetic complex. In the latter, the major part of the spin is on the N(NO) 2p orbital, with smaller contributions from the O(NO) 2p and Fe 3d. In tetracyanonitrosylferrate(I), the net charge on Fe is actually somewhat larger than the formal value +1, and the charge on N(NO) is more negative than in the pentacyano complexes. In sharp contrast to the case of $[Fe(CN)_5NO]^{3-}$, in $[Fe(CN)_4NO]^{2-}$ the spin is localized almost 90% on the Fe 3d orbital, with significant contribution from the 4p. The magnetic moments on NO have a non-negligible fraction on the N 2s, and the N and O 2p spins are coupled antiferromagnetically to the Fe moment.

In Fig 4 are displayed the energies of the molecular orbitals of the same complexes. In Table III are given the populations of the orbital of the unpaired electron in the Fe paramagnetic complexes. Examination of the tables and figure reveal that the unpaired electron in $[Fe(CN)_5NO]^{3-}$ is localized in a molecular orbital (the HOMO) constituted primarily of 2p(π) atomic orbitals of N and O (π^* (NO)), and to a lesser extent on the $3d_{xz}$ and $3d_{yz}$ orbitals of Fe. The HOMO is derived from the lowest unoccupied orbital of $[Fe(CN)_5NO]^{2-}$ (LUMO); however, in the latter diamagnetic complex there is an almost degeneracy of the LUMO (which would be a doubly-degenerate *e* orbital in C_{4v} symmetry) due to the approximate linearity of the Fe–NO bond. The bending of the Fe–N–O angle lifts this degeneracy, and thus the splitting of the *e* level may be viewed as a Jahn-Teller splitting. In Fig. 5 is depicted the variation of the orbital energies of $[Fe(CN)_5NO]^{3-}$ with θ, showing the increased splitting of the *e* levels as θ is increased. Variation of this angle affects the energies of the other levels less significantly.

On the other hand, the unpaired electron of the tetracyanonitrosylferrate(I) ion is localized primarily on the $3d_z^2$ orbital of Fe, with some contribution from Fe $4p_z$, N 2s, and N and O $2p_z$. Thus the spin is mainly distributed in a σ bond along the Fe–NO molecular axis. In both cases, some spin polarization of the inner valence shells is perceived clearly in the spin splittings in the energy levels diagrams. This polarization is larger in $[Fe(CN)_4NO]^{2-}$, due to the smaller difference in energy (and thus greater proximity of the spatial functions) between the HOMO and the nearest occupied valence levels. The spin polarization of the inner valence shells results in a somewhat different total spin magnetic moment distribution in the complex, as compared to the spin distribution in the HOMO.

The splitting of the *e* level (LUMO) in the paramagnetic pentacyanonitrosylferrate(I) due to the bending of the Fe–N–O angle (Jahn-Teller) is smaller than the spin splitting of the same orbital (see Fig. 4). In tetracyanonitrosylferrate(I), the absence of the fifth CN ligand opposite to NO results in a considerable weakening of the σ bond formed by Fe $3d_z^2$, which becomes localized in a smaller group of atoms (Fe-NO). As a consequence, the energy of the antibonding orbital containing Fe $3d_z^2$ (a_1 in C_{4v} symmetry) falls drastically, becoming lower than the energy of the *e* - derived orbitals located on π^* (NO). The same lowering of the crystal-field a_1 level energy was observed in molecular orbitals calculations with the present method for $[M(CN)_5]^{3-}$ (M=Co, Rh, Ir), which have a square-pyramidal structure similar to $[Fe(CN)_4NO]^{2-}$, in which the lower axial CN ligand is absent [38].

These results elucidate quite definitely the controversy on the nature of the orbital of the unpaired electron in $[Fe(CN)_5NO]^{3-}$, as described in the Introduction. This orbital forms a π bond between mainly π^* (NO) and Fe $3d_{xz}$, $3d_{yz}$. For this electron to be in a σ orbital localized mainly on Fe $3d_z^2$, as suggested in ref.[19], it is necessary that the axial CN be absent, as is the case in $[Fe(CN)_4NO]^{2-}$.

In Fig. 6 is illustrated the variation of the populations of the HOMO with θ. As the angle decreases, the contributions of the $2p_x$ and $2p_y$ orbitals of N, which form a π bond with Fe, decrease, and the $2p_z$ of N and O (which at 90^0 form a π bond of NO, as shown in Fig. 7) increase. The energy of the HOMO is stabilized with respect to its counterpart in the *e* - symmetry pair because it describes the bond of partially σ nature formed between the O $2p_z$ and the Fe orbitals, mainly with a combination of $3d_{xz}$ and $3d_{yz}$ (see Fig. 7). For all values of θ between 180 and 90^0, the $3d_z^2$ population of Fe remains low.

In Fig. 8 are given contour plots of the orbital of the unpaired electron for $[Fe(CN)_5NO]^{3-}$ and $[Fe(CN)_4NO]^{2-}$. The different nature of the bonds, π for pentacyanonitrosylferrate(I) and σ for tetracyanonitrosylferrate(I), is clearly seen in the maps. In the former, the orbital is antibonding between Fe and N, and between N and O; in the latter, it is mostly bonding between N and O and antibonding between Fe and N.

In Table IV are given the populations, charges and magnetic moments of $[Ru(CN)_5NO]^{2-}$ and $[Ru(CN)_5NO]^{3-}$. No report on the latter has been found in the literature; however, it has recently been identified by EPR after irradiation of the diamagnetic complex by 2 MeV electrons in a NaCl matrix [39]. The general features are similar to those of the corresponding Fe complexes, except that the positive charges on Ru are significantly higher than those on Fe. In Table V the

populations of the HOMO of $[Ru(CN)_5NO]^{3-}$ are discriminated. Again, no important differences from $[Fe(CN)_5NO]^{3-}$ are observed. The energies of the molecular orbitals of $[Ru(CN)_5NO]^{2-}$ and $[Ru(CN)_5NO]^{3-}$ are depicted in Fig. 9, and a contour map of the HOMO of the paramagnetic complex is shown in Fig. 10. The contours of the orbital of the unpaired electron are similar to the analogous Fe complex, except that in pentacyanonitrosylruthenate(I) the internal node of the Ru 4d radial function is clearly seen in the figure.

IV Mössbauer Quadrupole Splitting and Magnetic Hyperfine Tensor

The isotopes ^{57}Fe and ^{99}Ru are suitable for Mössbauer effect experiments in compounds of these elements. As mentioned in the Introduction, Mössbauer spectroscopy measurements were reported for $[Fe(CN)_5NO]^{2-}$, $[Fe(CN)_5NO]^{3-}$ and $[Fe(CN)_4NO]^{2-}$ [4]-[6]
and for $[Ru(CN)_5NO]^{2-}$ [13]. We have calculated the Quadrupole Splittings (ΔEQ) for these complexes, utilizing the self-consistent valence charge densities $\rho(\mathbf{r})$, with the expressions [40]

$$\Delta EQ = \tfrac{1}{2}\, e\, V_{zz}\, Q\, (1 + \eta^2/3)^{1/2} \qquad (5)$$

where Q is the quadrupole moment of the nucleus in the excited state of the Mössbauer transition , V_{zz} the principal component of the electric-field gradient tensor and η the asymmetry parameter given by $(V_{xx} - V_{yy})/V_{zz}$. The components of the electric-field gradient traceless tensor V_{ij} are given by (in atomic units) [41]:

$$V_{ij} = -\int \rho(\mathbf{r})\, (3x_i x_j - \delta_{ij}\, r^2)/r^5\, d\mathbf{r} + \sum_q Z_q^e\, (3x_{qi}x_{qj} - \delta_{ij}\, r^2)/r^5_q \qquad (6)$$

where the first term is the electronic component and the second term the point-charge contribution of the nuclei of the atoms surrounding the probe, screened by the core electrons and having effective nuclear charge Z_q^e .

After diagonalization of the tensor, the values of V_{xx} , V_{yy} and V_{zz} are obtained and employed in the calculation of ΔEQ and η, after redefining the diagonal elements according to the convention $|V_{zz}| > |V_{yy}| \geq |V_{xx}|$.

For ^{57}Fe, the value of Q (0.16b) has been determined by combining first-principles calculations of the electric-field gradients of a series of compounds with experimental values of ΔEQ [42]; for ^{99}Ru, we have adopted the value Q = 0.34b [43], [44].

The magnetic hyperfine coupling tensor is defined by the spin Hamiltonian [45], [46]

$$H = I \bullet A \bullet S \tag{7}$$

For the present complexes, S = 1/2. The first-order terms of the perturbation expansion of A are the Fermi (or contact} component A_F and the dipolar terms. A_F is defined as

$$A_F = 8\pi/3\ g_e\ \mu_B\ g_N\ \mu_N\ [\ \rho\uparrow(0) - \rho\downarrow(0)\ ] \tag{8}$$

where g_e and g_N are the electronic and nuclear spectroscopic factors, respectively, μ_B the Bohr magneton and μ_N the nuclear magneton. The first-order dipolar terms are given by

$$A_{ij}^{D} = g_e\ \mu_B\ g_N\ \mu_N \int [\ \rho\uparrow(\mathbf{r}) - \rho\downarrow(\mathbf{r})\ ]\ (3x_ix_j - \delta_{ij}\ r^2\ )/r^5\ d\mathbf{r} \tag{9}$$

After diagonalization of A^D, the components of the tensor are

$$A_{ii} = A_F + A_{ii}^{D}\ . \tag{10}$$

Second order terms may be neglected when the probe is a small atom, due to the small spin-orbit constant, although they may be quite important for transition elements [38]. Although the A_{ij} are given in units of energy (usually cm^{-1}), EPR spectroscopists frequently employ units of Gauss for the hyperfine tensor, by dividing by $g_e\ \mu_B$.

In the calculations of A_F , the 1s core contribution of N was obtained separately by atomic DFT calculations for the free ion, in the configuration that it has in the complex.

In Table VI are displayed the theoretical values of the quadrupole splittings and asymetry parameters for the five complexes. All calculated values compare quite well with the available experimental data, in the case of the Fe compounds. For $[Fe(CN)_4NO]^{2-}$, we compared the calculated value with the experimental value reported by Oosterhuis and Lang [6], for the complex

identified as $[Fe(CN)_5NOH]^{2-}$ by these authors and by van Voorst and Hemmerich [20]. In this, we followed the reinterpretation made by Schmidt et al. [6], who proposed that the blue reduction product is actually tetracyanonitrosylferrate(I). The good agreement between the theoretical and experimental values and, in particular, the correct sign obtained for the calculated ΔEQ, is further proof that the blue reduced complex is really $[Fe(CN)_4NO]^{2-}$.

For $[Ru(CN)_5NO]^{2-}$, the sign of ΔEQ was not measured, but it is reasonable to suppose that it is the same as $[Fe(CN)_5NO]^{2-}$. The less good accord of the theoretical value with experiment could be due to uncertainty in the value of Q (^{99}Ru) , and to the non-relativistic approximation employed.

In Table VII are displayed the theoretical and experimental values of the components of the magnetic hyperfine tensor at the N of the NO ligand for the paramagnetic complexes. The total valence spin densities on a plane containing the nuclei of the axial N-C-Fe-N-O atoms of $[Fe(CN)_5NO]^{3-}$ and Fe-N-O of $[Fe(CN)_4NO]^{2-}$ are plotted in Fig.11, and of $[Ru(CN)_5NO]^{3-}$ in Fig. 12. Most of the spin density is derived from the HOMO, although some polarization of the inner valence shells is present. The different nature of the HOMO of the pentacyano and tetracyano complexes is reflected in the spin densities: this is mostly of π symmetry in $[Fe(CN)_5NO]^{3-}$, and σ in $[Fe(CN)_4NO]^{2-}$. In the former complex, most of the spin density is positive, with a few lines of negative spin among the atoms. In the latter, the negative spin density which results on the N and O 2p negative magnetic moments (see Table II) is seen to have p(π) symmetry, and therefore does not pertain to the HOMO, where N and O contribute with $2p_z$ (see Table III and Fig 8). This negative spin density on N and O is therefore due to polarization (mostly by the Fe 3d moment) of the inner valence molecular orbitals..

Analysing Table VII, we observe large differences between the values for $[Fe(CN)_5NO]^{3-}$ and $[Fe(CN)_4NO]^{2-}$. The dipolar contributions are much larger in the former than in the latter. This may be associated to the much larger magnetic moment of the N_{NO} 2p orbital in the pentacyano complex, as seen in Table II. In all cases, the A_{33}^{D} is approximately in the *z* direction, i. e. , the Fe-N direction in our coordiante system; therefore, it may be identified approximately with $A_{||}$, and the other two components with $A_{\perp}$. The large anysotropy in the $A_{\perp}$ components of $[Fe(CN)_5NO]^{3-}$ is due to the bending of the Fe-N-O angle. This feature is not present in the tetracyano complex, where the same angle is near 180^{o} .

The Fermi or contact term is proportional to the spin density at the N nucleus, as defined in Eq. 8. In the non-relativistic approximation, only s electrons penetrate the nucleus. The 1s electrons

are polarized by the valence spin moments, and thus contribute to A_F , in spite of the fact that they are in a complete shell. In $[Fe(CN)_5NO]^{3-}$, the contribution of the 1s is negative, since it is the result of the polarization of the core electrons by the large positive 2p moment on N (see Table II). The majority spin up electrons on the 2p attract the 1s electrons of the same spin through the exchange forces in the direction of the valence region, leaving behind electronic density of the opposite spin, which thus occupies the nucleus preferentially. On the contrary, in $[Fe(CN)_4NO]^{2-}$ the 1s contribution is positive, since the 2p moment of N is negative. The valence contribution is positive in all cases; although these functions are also polarized by the valence moments, this is primarily the direct result of positive magnetic moments on the N 2s, present in all paramagnetic complexes (see Tables II and IV). Since the value of the N 2s moment is considerably higher in the tetracyano complex , the valence contribution to the spin density is much larger in this complex, and adds to the positive core term, resulting in a very large positive Fermi hyperfine constant.

Comparison with experiment may be done with the data compiled in Table VII. The experimental values obtained by EPR spectroscopy have undetermined signs. The agreement between theoretical and experimental values for $[Fe(CN)_5NO]^{3-}$ is fairly good. For $[Fe(CN)_4NO]^{2-}$, calculated values are higher than those measured. The most probable explanation for this discrepancy is that the hyperfine constants of the pentacyano complex are dominated by the dipolar terms, due to the large N 2p population, and these terms are obtained via an integral involving the spin density over all space (Eq. 9). On the contrary, in $[Fe(CN)_4NO]^{2-}$ the hyperfine constants are primarily derived from the Fermi contribution, which depends on the spin density at one point in space and thus is much more sensitive to detailed features of the electron distribution, and therefore to the exchange-correlation potential employed. The local density approximation, which was used here in the self-consistent step of the calculations, is known to deplete the electron density of the core region of centers such as O in molecules, in favor of the valence region, as compared to gradient-corrected nonlocal potentials [47]. Therefore, one may speculate that the large valence contribution to A_F in the tetracyano complex has been overestimated in the present calculation. However, DFT calculations of the contact term in the O of H_2O, performed with several different nonlocal exchange-correlation functionals, gave a variety of very different values, ranging from +0.6 to -24.6 Gauss [48]. Therefore, we sustain that more systematic studies on the effect of nonlocal potentials on the electron and spin densities are needed, before it is concluded that that one or more forms constitute an improvement over the local approximation.

Although quantitative agreement is not obtained, some features of the calculated values for $[Fe(CN)_4NO]^{2-}$ coincide with experiment. The values of $A_\perp$ are very similar, due to the almost

tetragonal symmetry of the complex; A_{33} (the component along the Fe-N-O direction) is the largest component. The value of A_{ISO} , which we may identify as A_F , is of the same order of all A_{ii}, which agrees with our result that it is the dominant component.

The results for $[Ru(CN)_5NO]^{3-}$ are very similar to those for its Fe counterpart, as is the spin density contour map (Fig. 12), and are given here as a prediction for future EPR measurements.

V. Conclusions

In summary, the Density Functional calculations reported here have enlightened many aspects of the electronic structure, magnetism and hyperfine properties of the covalent Fe and Ru complexes investigated. A long-standing controversy on the ground-state configuration of $[Fe(CN)_5NO]^{3-}$, a reduction product of nitroprusside, has been elucidated, and the unpaired electron was found to be in a molecular orbital constituted primarily of π^* (NO). In addition, total energy caculations revealed that the Fe-N-O bond is bent, with angle of 152.5^o . Increased evidence has been found for the identification of another reduction product, which is blue in solution, as the complex $[Fe(CN)_4NO]^{2-}$, with the unpaired electron in an orbital primarily on $3d_z^2$ of Fe. Further corroboration for these conclusions was obtained by the good agreement between calculated and experimental values of the Mössbauer quadrupole splittings on Fe for these complexes, as well as for nitroprusside. Calculations of magnetic hyperfine coupling constants give a fair accord with experiment, and corroborate the conclusions drawn. The calculations were extended to the Ru complexes $[Ru(CN)_5NO]^{2-}$ and $[Ru(CN)_5NO]^{3-}$, and for the latter predictions of quadrupole splittings and hyperfine coupling constants were made.

Aknowledgements

The authors are grateful to N. V. Vugman for bringing to their attention this fascinating subject. Calculations were performed partly at the Cray J90 of the Supercomputing Center of the Universidade Federal do Rio Grande do Sul.

TABLE CAPTIONS

Table I

Interatomic distances and angles in the M-N-O bond of nitrosyl complexes.

a) From reference [2]

b) From reference [12]

c) Theoretical values, this work.

Table II

Mulliken populations, magnetic moments and net charges of Fe complexes. Net charges are defined as (Z − total population), where Z is the atomic number. C_{eq} and N_{eq} are equatorial (CN) C and N, respectively. C_{ax} and N_{ax} are axial (CN) C and N, respectively. For C_{eq} and N_{eq} , values are averages of equatorial C and N atoms.

Table III

Distribution of the unpaired electron in the HOMO of paramagnetic Fe complexes. For C_{eq} and N_{eq} , values are averages of equatorial C an N, respectively.

Table IV

Mulliken populations, magnetic moments and net charges of Ru complexes. Net charges are defined as (Z − total population), where Z is the atomic number. C_{eq} and N_{eq} are equatorial (CN) C and N, respectively. C_{ax} and N_{ax} are axial (CN) C and N, respectively. For C_{eq} and N_{eq} , values are averages of equatorial C and N atoms.

TABLE V

Distribution of the unpaired electron in the HOMO of paramagnetic Ru complexes. For C_{eq} and N_{eq} , values are averages of equatorial C and N, respectively.

Table VI

Calculated and experimental quadrupole splittings ΔEQ at the metal site and assymetry parameters η .

a) Value of Q (^{57}Fe) = 0.16b (from ref. [42]); value of Q (^{99}Ru) = 0.34b (from refs. [43] and [44])

b) From ref. [4]

c) From ref. [6]

d) Assuming for this complex the value given in ref. [6] for $[Fe(CN)_5NOH]^{2-}$, see discussion in text.

e) From ref. [13a]

f) From ref. [13b]

Table VII

Theoretical and experimental values of the magnetic hyperfine coupling constants at the N of NO for Fe and Ru paramagnetic complexes (in Gauss).

a) g_N (^{14}N) = 0.40376

b) From ref. [20]

c) From ref. [21a]

Table I

	$[Fe(CN)_5NO]^{2-}$	$[Fe(CN)_5NO]^{3-}$	$[Ru(CN)_5NO]^{2-}$	$[Ru(CN)_5NO]^{3-}$
M-N distance (Å)	1.653[a]	1.735[c]	1.773[b]	1.855[c]
M-N-O angle (degree)	175.7[a]	152.5[c]	174.4[b]	144.0[c]

Table II

atomic orbital		$[Fe(CN)_5NO]^{2-}$		$[Fe(CN)_5NO]^{3-}$			$[Fe(CN)_4NO]^{2-}$		
		population	net charge	population	magnetic moment (μ_B)	net charge	population	magnetic moment (μ_B)	net charge
Fe	3s	1.944	1.086	1.949	0.000	0.934	1.936	0.000	1.290
	3p	5.936		5.941	0.001		5.935	–0.001	
	3d	6.503		6.594	0.167		6.374	0.869	
	4s	0.065		0.068	–0.002		0.046	0.003	
	4p	0.468		0.513	–0.008		0.420	0.128	
C_{ax}	2s	1.153	0.273	1.197	0.012	0.300	-	-	-
	2p	2.573		2.503	0.012		-	-	
C_{eq}	2s	1.186	0.253	1.224	0.004	0.282	1.224	0.000	0.171
	2p	2.562		2.495	0.002		2.606	–0.008	
N_{NO}	2s	1.627	0.051	1.633	0.021	–0.003	1.661	0.057	–0.183
	2p	3.322		3.370	0.593		3.522	–0.136	
O_{NO}	2s	1.829	–0.222	1.822	–0.003	–0.387	1.835	–0.004	–0.265
	2p	4.393		4.566	0.198		4.430	–0.055	
N_{ax}	2s	1.753	–0.822	1.757	0.000	–0.980	-	-	-
	2p	4.069		4.223	0.000		-	-	
N_{eq}	2s	1.755	–0.844	1.750	0.000	–0.998	1.761	0.000	–0.881
	2p	4.090		4.249	–0.003		4.120	0.042	

Table III

$[Fe(CN)_5NO]^{3-}$	$[Fe(CN)_4NO]^{2-}$

atomic orbital		population	atomic orbital		Population
Fe 3d	xy	0.000	Fe 3d	xy	0.000
	yz	0.119		yz	0.001
	z^2	0.022		z^2	0.509
	xz	0.116		xz	0.001
	x^2-y^2	0.000		x^2-y^2	0.000
Fe 4s		0.000	Fe 4s		0.000
Fe 4p	y	0.001	Fe 4p	y	0.000
	z	0.000		z	0.160
	x	0.001		x	0.000
N_{NO} 2s		0.014	N_{NO} 2s		0.056
N_{NO} 2p	y	0.173	N_{NO} 2p	y	0.000
	z	0.062		z	0.014
	x	0.165		x	0.000
O_{NO} 2s		0.000	O_{NO} 2s		0.000
O_{NO} 2p	y	0.108	O_{NO} 2p	y	0.000
	z	0.025		z	0.023
	x	0.103		x	0.000
C_{ax}	2s + 2p	0.024	C_{eq}	2s + 2p	0.022
C_{eq}	2s + 2p	0.010	N_{eq}	2s + 2p	0.037
N_{ax}	2s + 2p	0.012			
N_{eq}	2s + 2p	0.004			

Table IV

	$[Ru(CN)_5NO]^{2-}$		$[Ru(CN)_5NO]^{3-}$		
atomic orbital	population	net charge	population	magnetic moment (μ_B)	net charge
Ru 4s	1.933	1.709	1.938	0.001	1.584
4p	5.895		5.906	0.002	
4d	6.099		6.214	0.120	
5s	0.066		0.060	–0.002	
5p	0.298		0.296	–0.006	
C_{ax} 2s	1.198	0.192	1.229	0.016	0.206
2p	2.611		2.565	0.022	
C_{eq} 2s	1.216	0.177	1.260	0.003	0.179
2p	2.607		2.561	0.004	
N_{NO} 2s	1.634	–0.007	1.650	0.017	–0.120
2p	3.435		3.470	0.560	
O_{NO} 2s	1.828	–0.235	1.820	–0.003	–0.378
2p	4.407		4.558	0.228	
N_{ax} 2s	1.756	–0.848	1.753	0.000	–0.991
2p	4.092		4.238	0.008	
N_{eq} 2s	1.755	–0.864	1.749	0.000	–1.005
2p	4.109		4.256	0.003	

Table V

$[Ru(CN)_5NO]^{3-}$

atomic orbital		Population
Ru 4d	xy	0.001
	yz	0.114
	z^2	0.014
	xz	0.110
	x^2-y^2	0.000
Ru 5s		0.000
Ru 5p	y	0.000
	z	0.000
	x	0.000
N_{NO} 2s		0.014
N_{NO} 2p	y	0.138
	z	0.103
	x	0.129
O_{NO} 2s		0.000
O_{NO} 2p	y	0.097
	z	0.049
	x	0.091
C_{ax}	2s+2p	0.035
C_{eq}	2s+2p	0.011
N_{ax}	2s+2p	0.024
N_{eq}	2s+2p	0.009

Table VI

Complex	Calculated[a]		Experimental	
	ΔEQ (mm/s)	η	ΔEQ (mm/s)	η
$[Fe(CN)_5NO]^{2-}$	+1.996	0.057	+1.726 (300K)[b] +1.82 (195K)[c] +1.90 (77K)[c]	0.00
$[Fe(CN)_5NO]^{3-}$	–1.159	0.252	–1.25 (195K)[c]	<0.5[c]
$[Fe(CN)_4NO]^{2-}$	+1.763	0.040	+2.02 (77K)[c,d]	0.0[c]
$[Ru(CN)_5NO]^{2-}$	+0.786	0.004	0.49[e] 0.40[f]	–
$[Ru(CN)_5NO]^{3-}$	–0.542	0.240	–	–

Table VII

Calculated[a]		$[Fe(CN)_5NO]^{3-}$	$[Fe(CN)_4NO]^{2-}$	$[Ru(CN)_5NO]^{3-}$
A_{11}^D		–9.578	–1.589	–8.566
A_{22}^D		+20.855	–1.667	+19.009
A_{33}^D		–11.277	+3.256	–10.443
A_F	1s	–13.293	+3.639	–12.333
	valence	+14.538	+21.825	+13.208
	Total	+1.245	+25.464	+0.875
A_{11}		–8.34	+23.88	–7.69
A_{22}		+22.10	+23.80	+19.88
A_{33}		–10.04	+28.72	–9.57
Experimental				
$A_\perp$		18.3, 25.9[b]	14.5, 14.5[c]	---
			14.75[b]	
$A_{\|\|}$		8.5[b]	16.9[c]	---
			17.1[b]	---
A_{ISO}		---	14.67[c]	---

FIGURE CAPTIONS

Figure 1

a) Representation of $[Fe(CN)_5NO]^{3-}$.

b) Representation of $[Fe(CN)_4NO]^{2-}$.

Figure 2

a) Total energy of $[Fe(CN)_5NO]^{3-}$ (in Hartree atomic units, arbitrary origin) against the Fe–NO distance d. Line is to guide the eye.

b) Total energy of $[Fe(CN)_5NO]^{3-}$ (in Hartree atomic units, arbitrary origin) against the Fe–N–O angle θ. Line is to guide the eye.

Figure 3

a) Total energy of $[Ru(CN)_5NO]^{3-}$ (in Hartree atomic units, arbitrary origin) against the Fe–NO distance d. Line is to guide the eye.

b) Total energy of $[Ru(CN)_5NO]^{3-}$ (in Hartree atomic units, arbitrary origin) against the Fe–N–O angle θ. Line is to guide the eye.

Figure 4

Molecular orbital energy levels of $[Fe(CN)_5NO]^{2-}$, $[Fe(CN)_5NO]^{3-}$ and $[Fe(CN)_4NO]^{2-}$. Major components of orbitals are indicated.

Figure 5

Variation of the molecular orbital energy levels of $[Fe(CN)_5NO]^{3-}$ with the Fe–N–O angle θ. The arrow identifies the HOMO. Dotted line indicates the equilibrium angle.

Figure 6

Variation of the populations of the MO of the unpaired electron (HOMO) of $[Fe(CN)_5NO]^{3-}$ with the Fe–N–O angle θ.

Figure 7

Schematics of atomic orbitals in $[Fe(CN)_5NO]^{3-}$, showing different interactions present at $\theta = 180^o$ and $\theta = 90^o$.

Figure 8

a) Contour map of the molecular orbital of the unpaired electron (HOMO) of $[Fe(CN)_5NO]^{3-}$ on the plane containing the axial NC–Fe–NO atomic nuclei. Contours are from 0.3 to 0.001 with intervals of 0.01 e/a_0^3 , and from –0.3 to –0.001 with intervals of 0.01 e/a_0^3. Thick lines are positive values, thin lines are negative values.

b) Contour map of the molecular orbital of the unpaired electron (HOMO) of $[Fe(CN)_4NO]^{2-}$ on the plane containing the Fe–NO atomic nuclei. Contours are from 0.5 to 0.001 with intervals of 0.01 e/a_0^3 , and from –0.5 to –0.001 with intervals of 0.01 e/a_0^3. Thick lines are positive values, thin lines are negative values.

Figure 9

Molecular orbital energy levels of $[Ru(CN)_5NO]^{2-}$ and $[Ru(CN)_5NO]^{3-}$. Major components of the orbitals are indicated.

Figure 10

Contour map of the molecular orbital of the unpaired electron (HOMO) of $[Ru(CN)_5NO]^{3-}$ on the plane containing the axial NC–Ru–NO atomic nuclei. Contours are from 0.3 to 0.001 with intervals of 0.01 e/a_0^3 , and from –0.3 to –0.001 with intervals of 0.01 e/a_0^3. Thick lines are positive values, thin lines are negative values.

Figure 11

a) Total valence spin density $[\rho\uparrow(\mathbf{r}) - \rho\downarrow(\mathbf{r})]$ contour map of $[Fe(CN)_5NO]^{3-}$ on the plane containing the axial NC–Fe–NO atomic nuclei. Contours are from 0.04 to 0.0001 with intervals of 0.001 e/a_0^3 , and from –0.04 to –0.0001 with intervals of 0.001 e/a_0^3. Thick lines are positive values, thin lines are negative values.

a) Total valence spin density $[\rho\uparrow(\mathbf{r}) - \rho\downarrow(\mathbf{r})]$ contour map of $[Fe(CN)_4NO]^{2-}$ on the plane containing the Fe–NO atomic nuclei. Contours are from 0.5 to 0.001 with intervals of 0.01 e/a_0^3 , and from –0.5 to –0.001 with intervals of 0.01 e/a_0^3. Thick lines are positive values, thin lines are negative values.

Figure 12

Total valence spin density $[\rho\uparrow(\mathbf{r}) - \rho\downarrow(\mathbf{r})]$ contour map of $[Ru(CN)_5NO]^{3-}$ on the plane containing the axial NC−Ru−NO atomic nuclei. Contours are from 0.04 to 0.0001 with intervals of 0.001 e/a_0^3, and from −0.04 to −0.0001 with intervals of 0.001 e/a_0^3. Thick lines are positive values, thin lines are negative values.

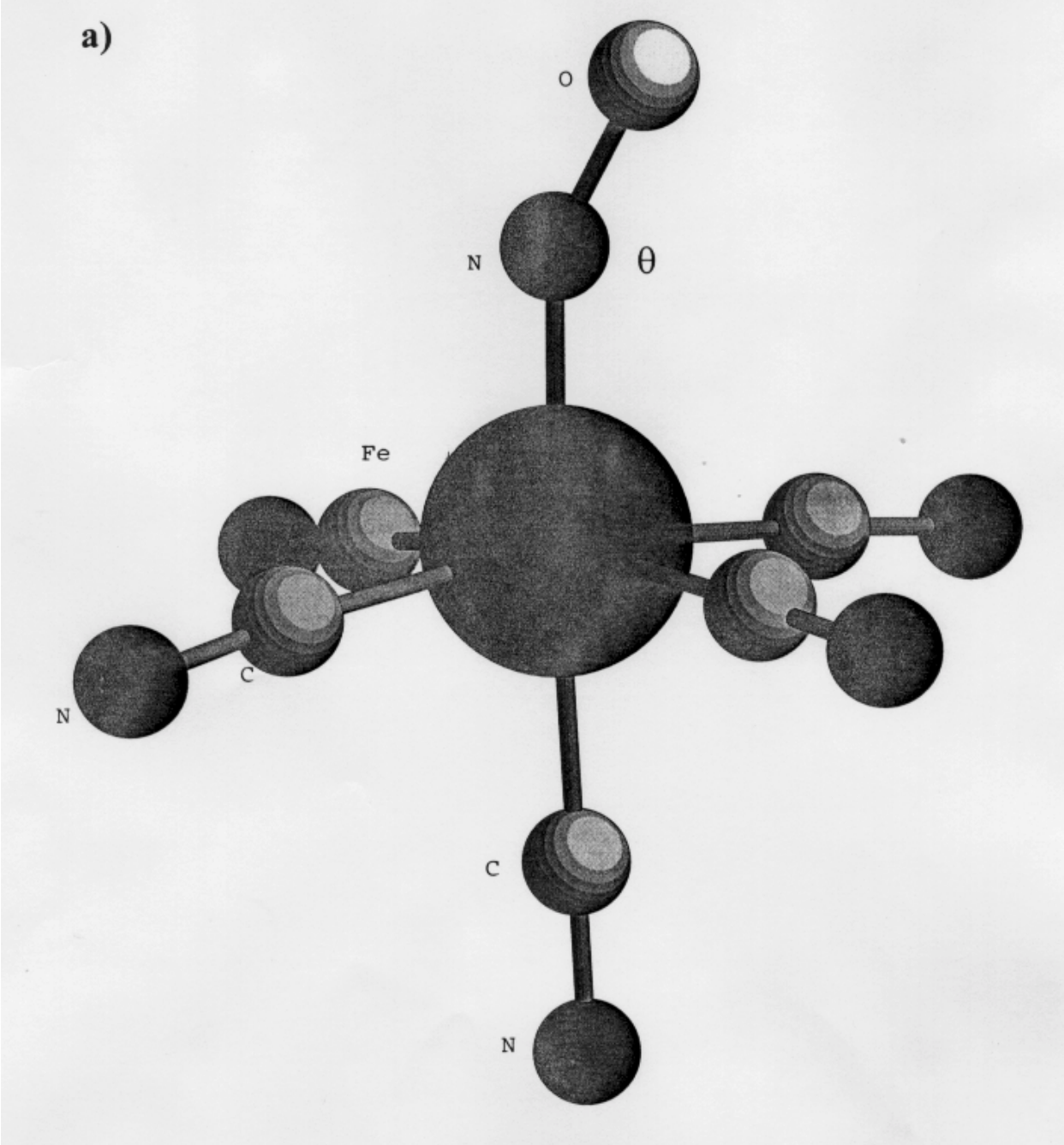

FIGURE 1a

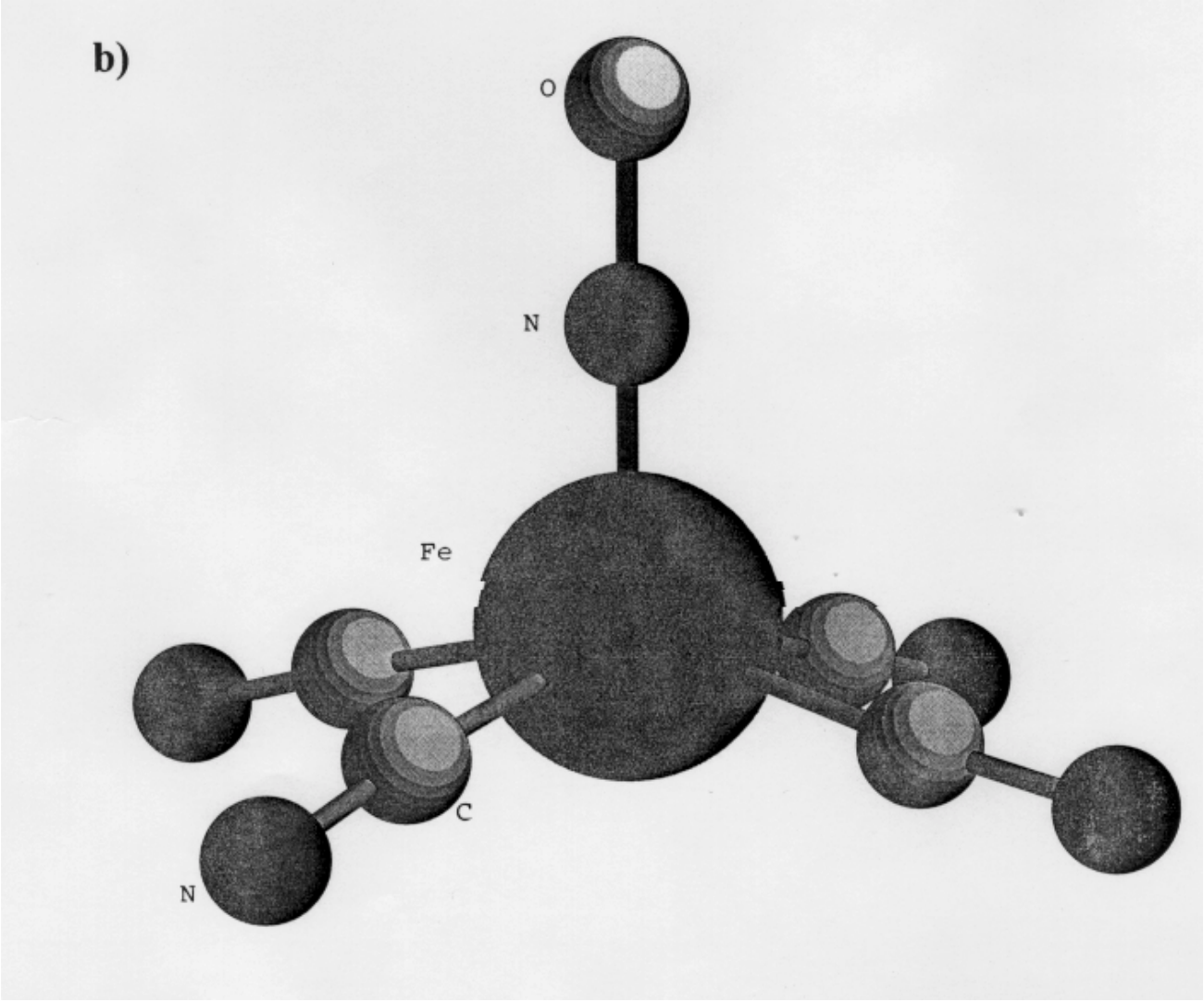

FIGURE 1b

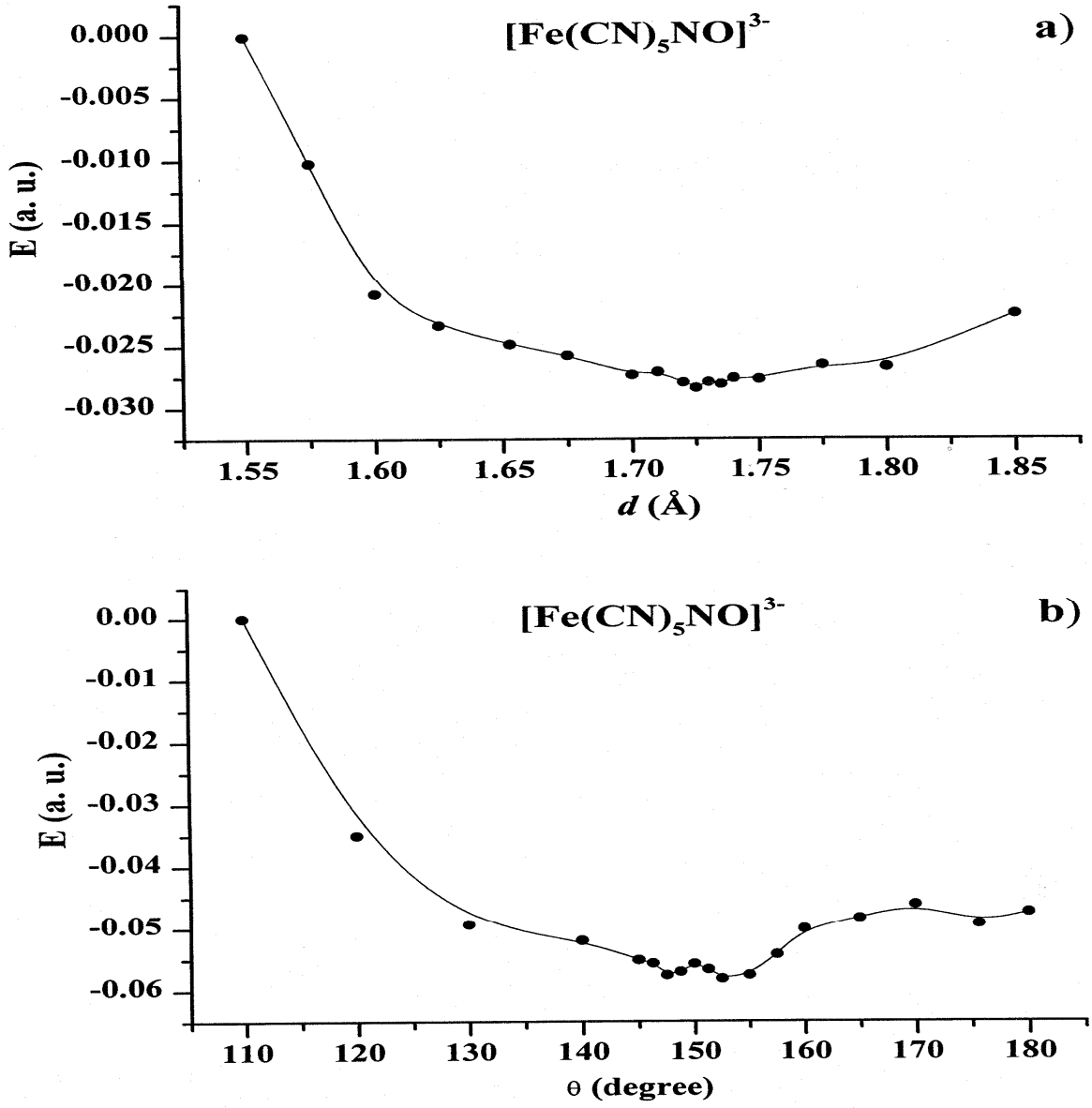
[Fe(CN)5NO]3-
a)
0.000
-0.005
-0.010
-0.015
-0.020
-0.025
-0.030
E (a. u.)
1.55
1.60
1.65
1.70
1.75
1.80
1.85
d (Å)
[Fe(CN)5NO]3-
b)
0.00
-0.01
-0.02
-0.03
-0.04
-0.05
-0.06
E (a. u.)
110
120
130
140
150
160
170
180
θ (degree)

FIGURE 2

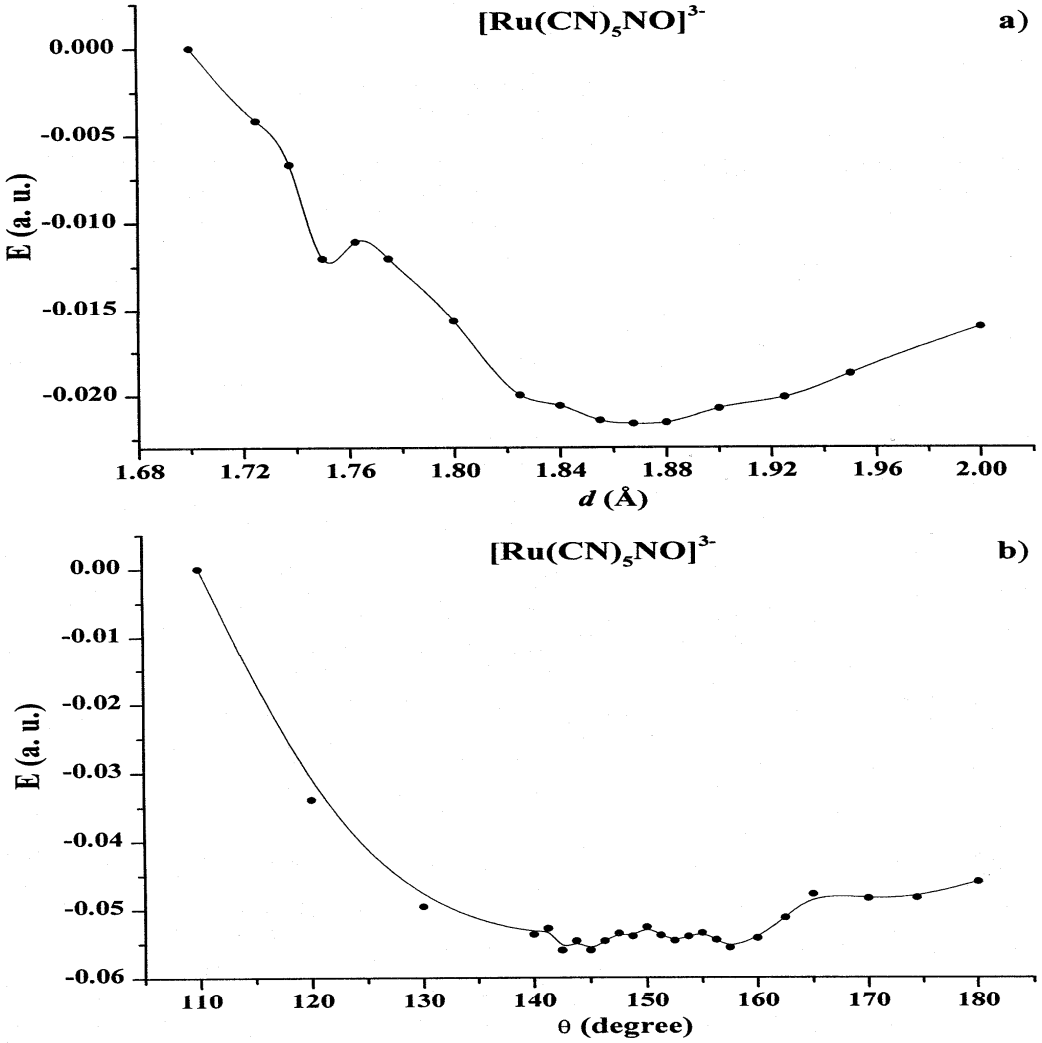
[Ru(CN)5NO]3-
a)
0.000
-0.005
-0.010
-0.015
-0.020
E (a. u.)
1.68
1.72
1.76
1.80
1.84
1.88
1.92
1.96
2.00
d (Å)
[Ru(CN)5NO]3-
b)
0.00
-0.01
-0.02
-0.03
-0.04
-0.05
-0.06
E (a. u.)
110
120
130
140
150
160
170
180
θ (degree)

FIGURE 3

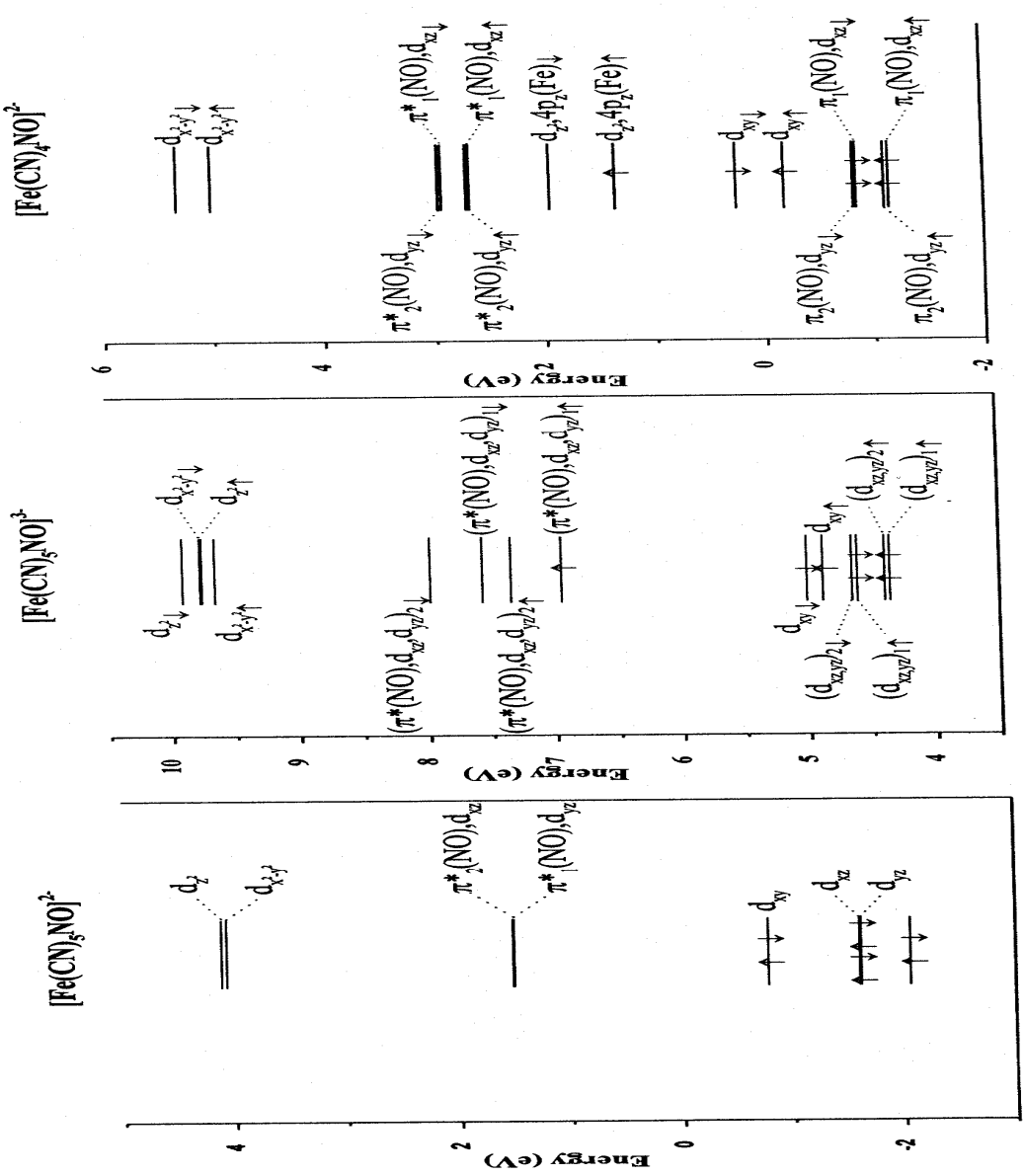

FIGURE 4

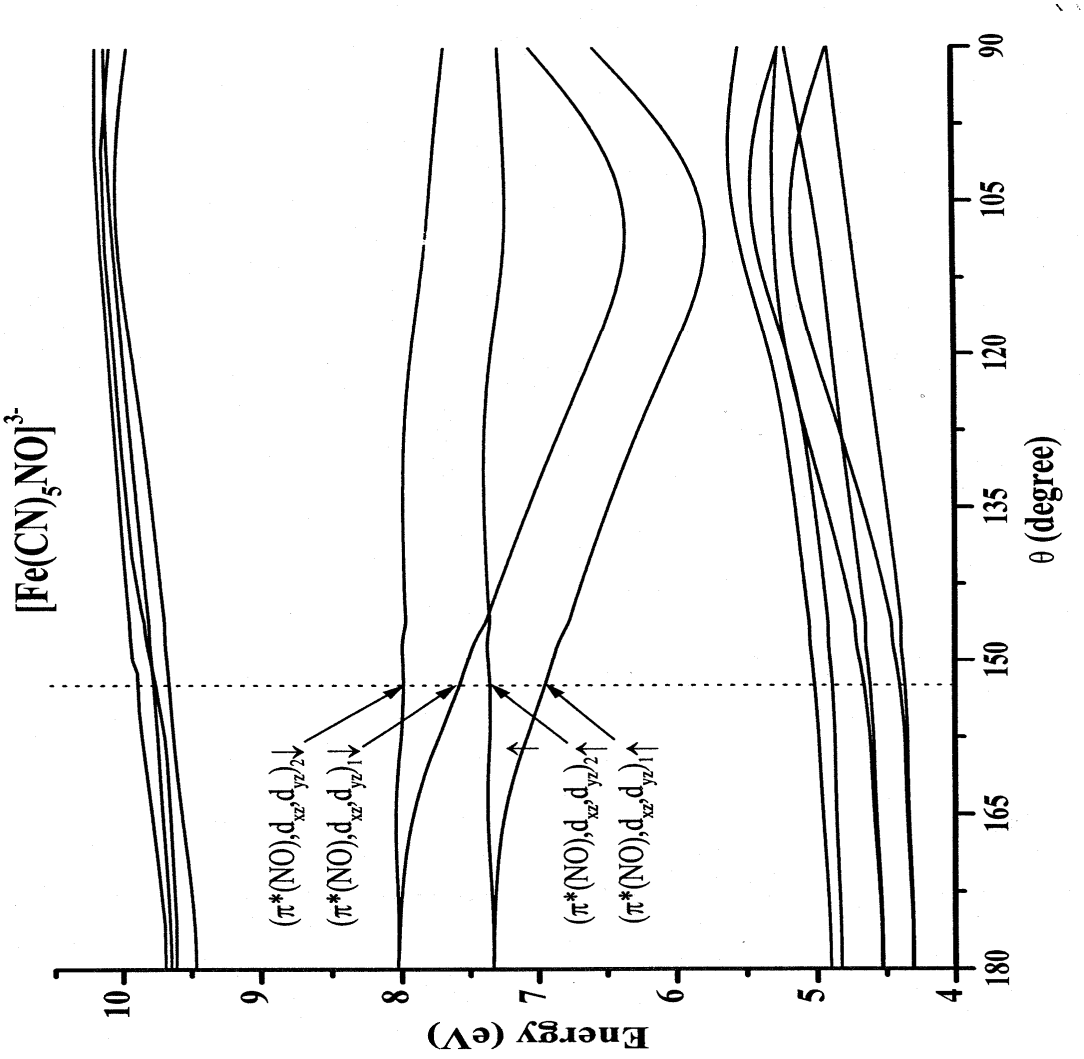
[Fe(CN)5NO]3-
Energy (eV)
θ (degree)
(π*(NO),dxz,dyz/2)↓
(π*(NO),dxz,dyz/1)↓
(π*(NO),dxz,dyz/2)↑
(π*(NO),dxz,dyz/1)↑

FIGURE 5

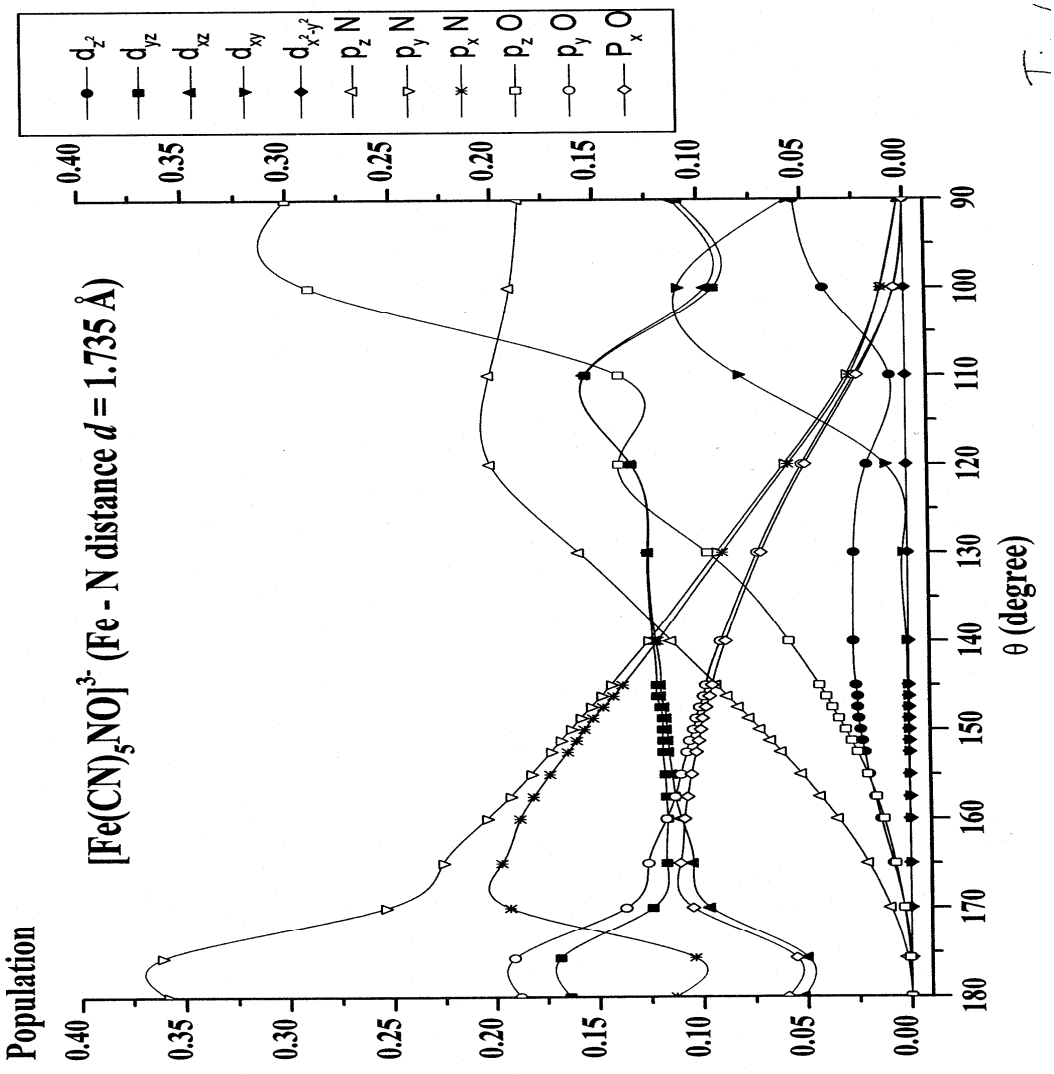
Population
[Fe(CN)5NO]3- (Fe - N distance d = 1.735 Å)
θ (degree)
dz2
dyz
dxz
dxy
dx2-y2
pz N
py N
px N
pz O
py O
Px O

FIGURE 6

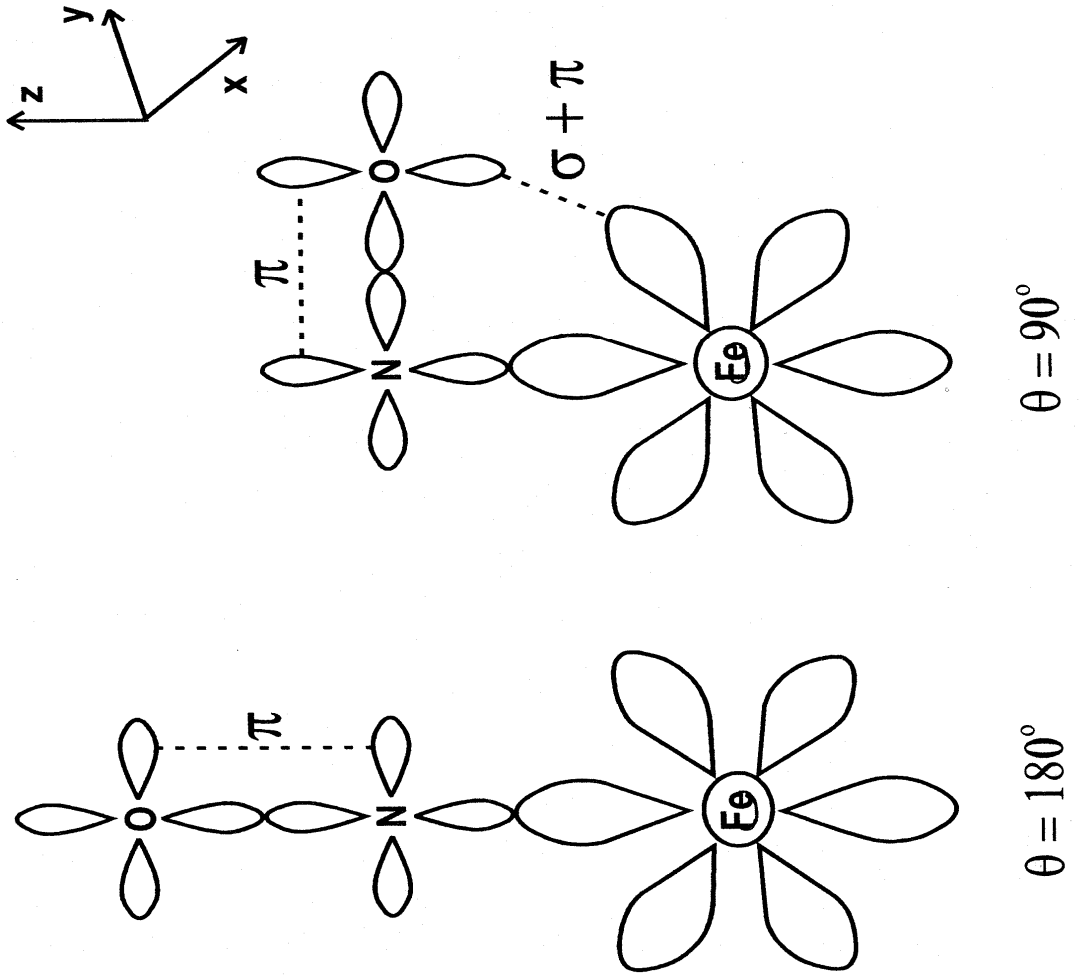

FIGURE 7

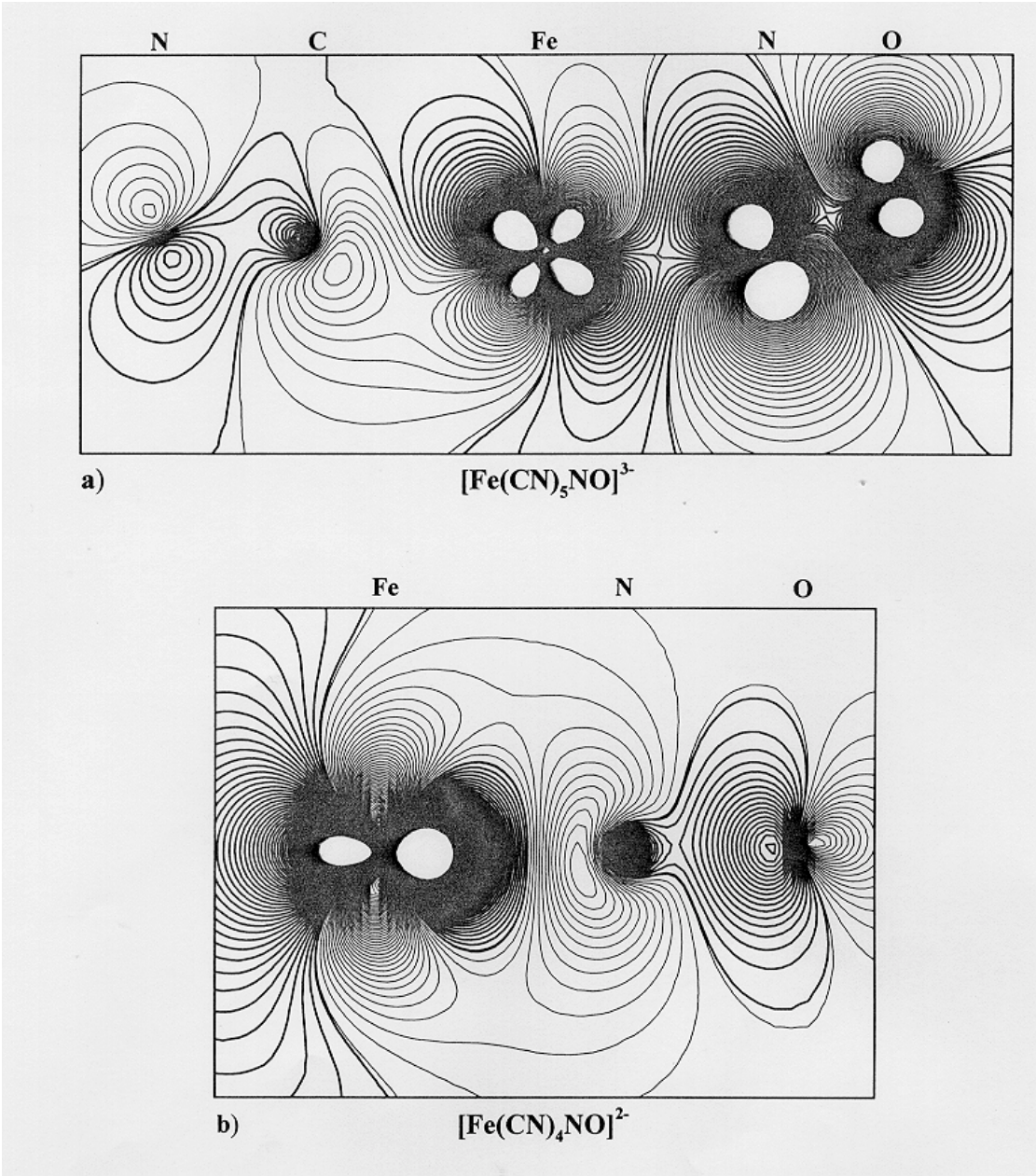

FIGURE 8

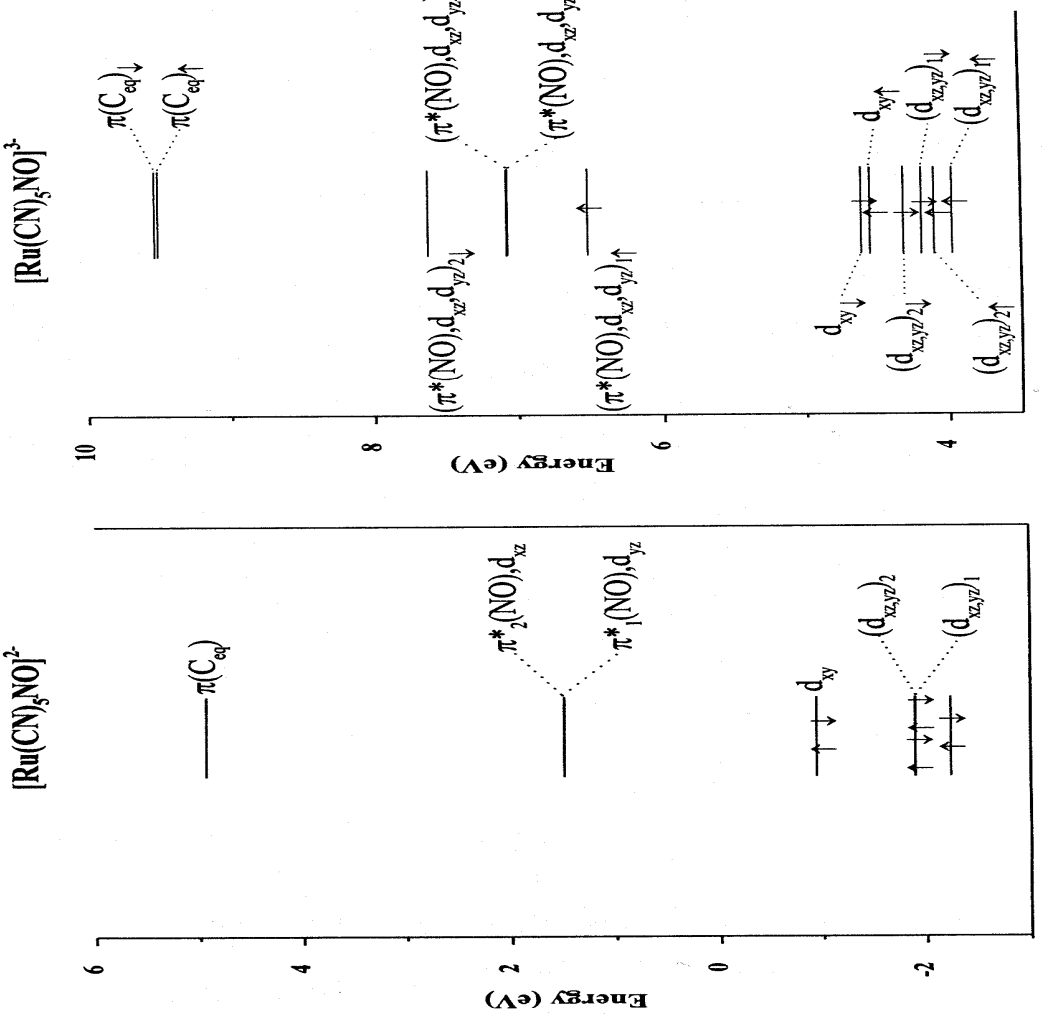
[Ru(CN)5NO]2-
[Ru(CN)5NO]3-
π(Ceq)
π*2(NO),dxz
π*1(NO),dyz
dxy
(dxz,yz)2
(dxz,yz)1
π(Ceq)↓
π(Ceq)↑
(π*(NO),dxz,dyz)1↓
(π*(NO),dxz,dyz)2↓
(π*(NO),dxz,dyz)1↑
dxy↓
dxy↑
(dxz,yz)2↓
(dxz,yz)1↓
(dxz,yz)2↑
(dxz,yz)1↑
Energy (eV)
Energy (eV)

FIGURE 9

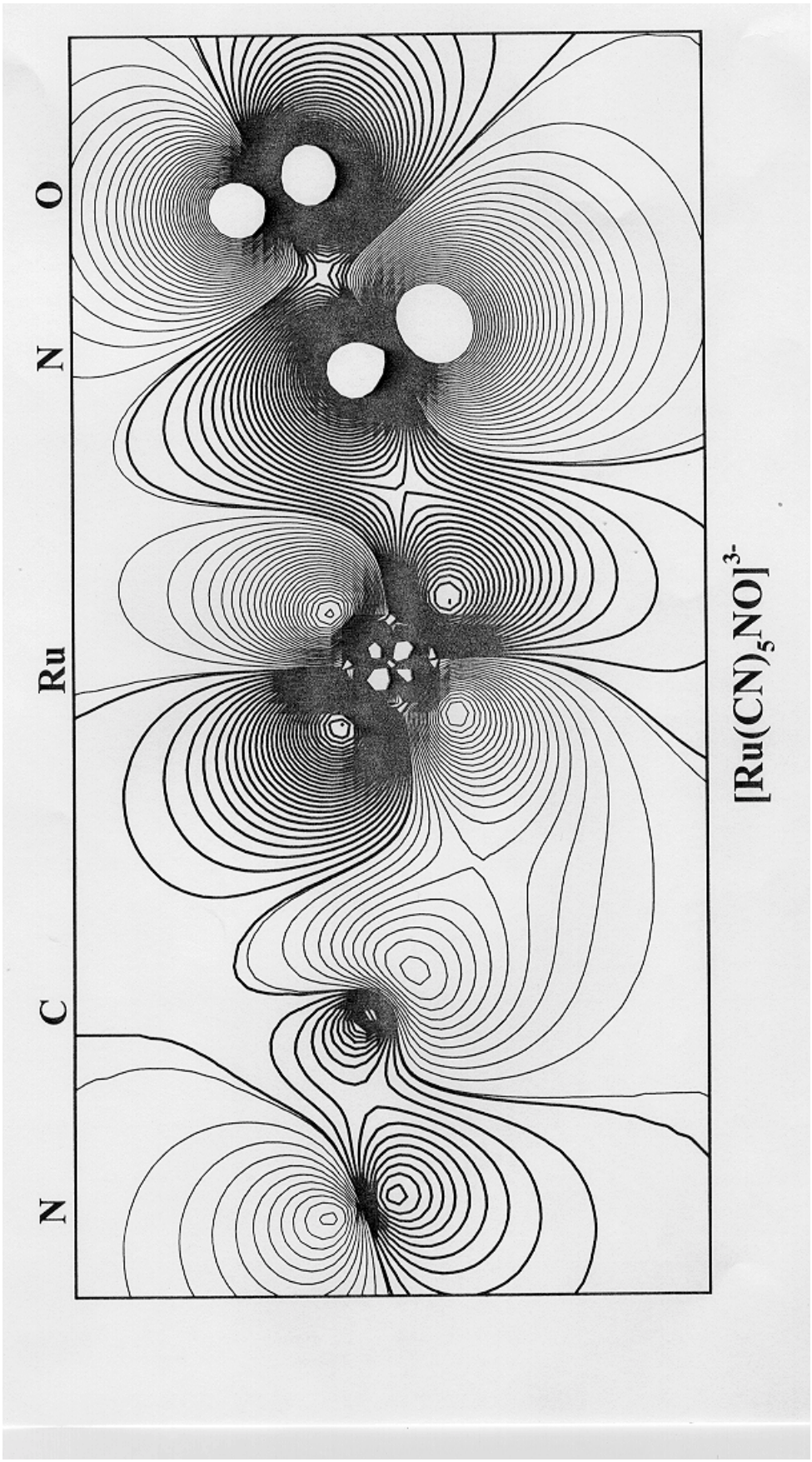

FIGURE 10

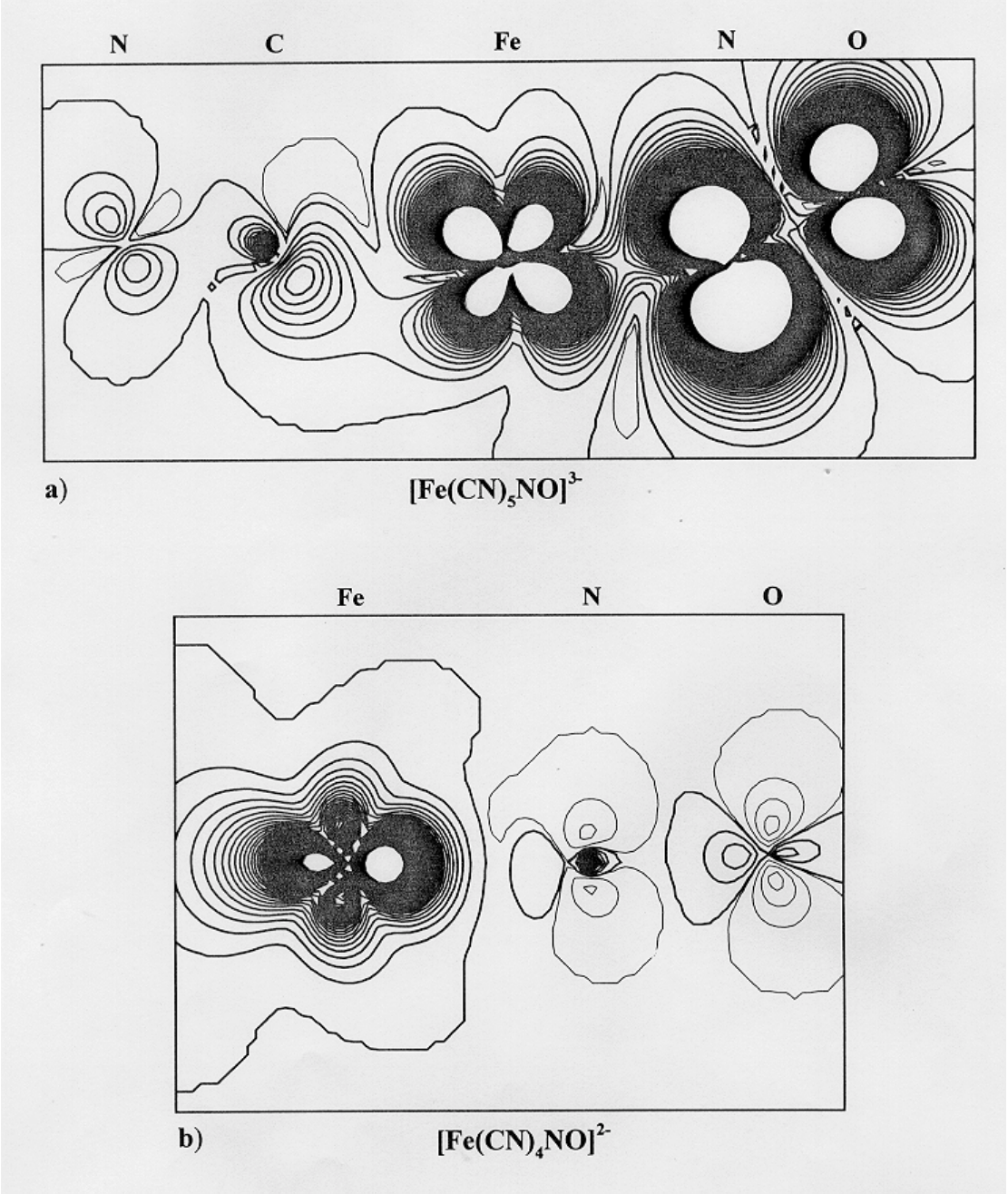

FIGURE 11

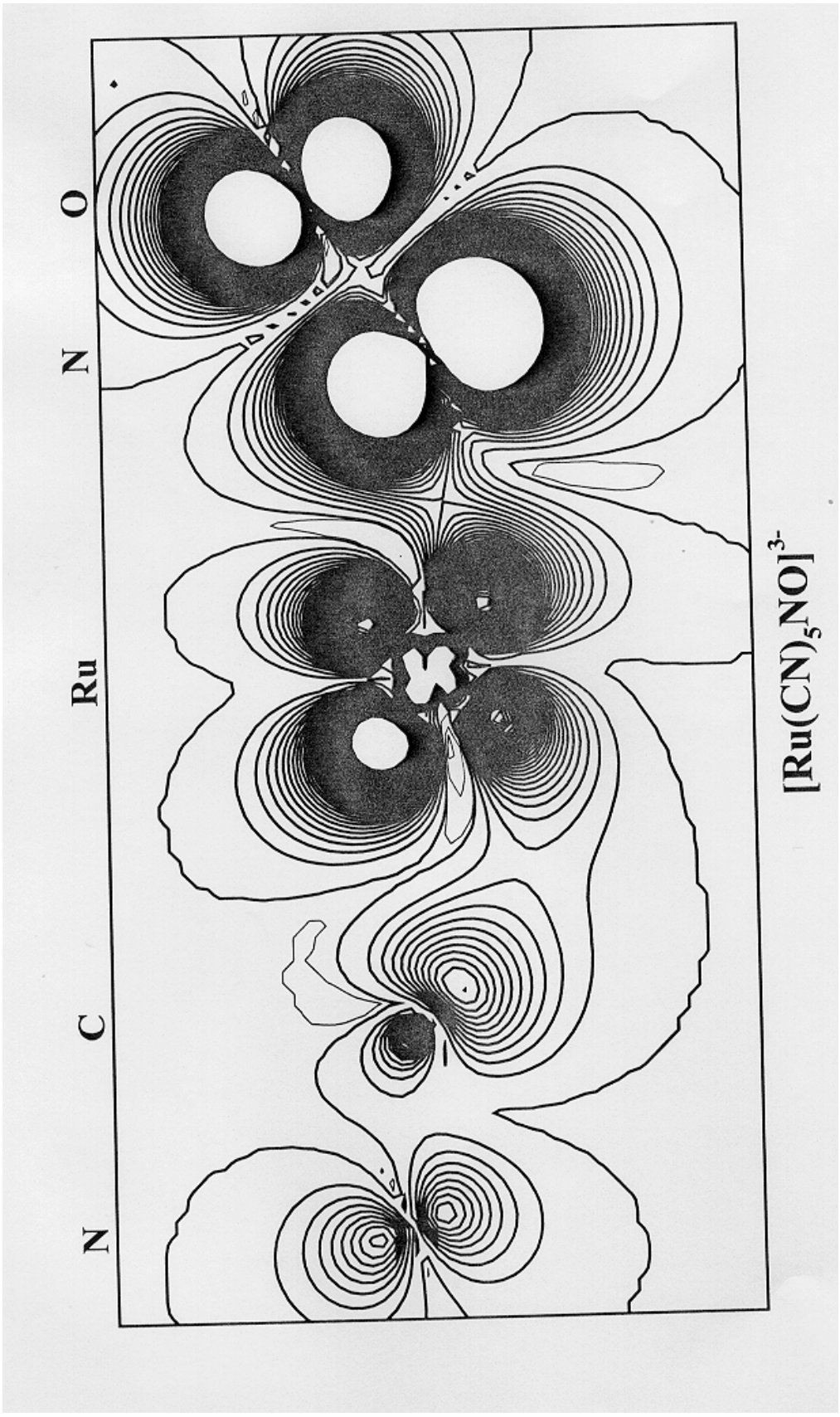

FIGURE 12

REFERENCES

1) P. T. Manoharan and H. B. Gray, J. Am. Chem. Soc. **87**, 3340 (1965)

2) F. Bottomley and P. S. White, Acta Cryst. **B35**, 2193 (1979)

3) M. D. Carducci, M. R. Pressprich and P. Coppens, J. Am. Chem. Soc. **119**, 2669 (1997)

4) J. Danon and L. Ianarella, J. Chem. Phys. **47**, 382 (1967)

5) W. A. Mundt and T. Sonino, J. Chem. Phys. **50**, 3127 (1969)

6) W. T. Oosterhuis and G. Lang, J. Chem. Phys. **50**, 4381 (1969)

7) J. A. Guida, O. E. Piro and P. J. Aymonino, Solid State Comm. **66**, 1007 (1988)

8) A. Navaza, G. Chevrier, P. M. Alzari and P. J. Aymonino, Acta Cryst. **C45**, 839 (1989); A. Navaza, G. Chevier, A. Gukasov and P. J. Aymonino, J. Solid. State Chem. **123**, 48 (1996)

9) V. I. Nefedov, Y. V. Salyn, A. P. Sadovsky and I. Beyer, J. Elec. Spec. Rel. Phen. **12**, 121 (1977)

10) D. A. Estrin, L. M. Baraldo, L. D. Slep, B. C. Barja, J. A. Olabe, L. Paglieri and G. Corongiu, Inorg. Chem. **35**, 3897 (1996)

11) D. Guenzburger, A. Garnier and J. Danon, Inorganica Chimica Acta **21**, 119 (1977)

12) J. A. Olabe, L. A. Gentil, G. Rigotti and A. Navaza, Inorg. Chem. **23**, 4297 (1984)

13) a) C. A. Clause, R. A. Prados and M. L. Good, J. Am. Chem. Soc. **92**, 7482 (1970); b) R. Greatex, N. N. Greenwood and P. Kaspi, J. Chem. Soc. A (**1971**), 1873

14) L. M. Baraldo, M. S. Bessega, G. E. Rigotti and J. A. Olabe, Inorg. Chem. **33**, 5890 (1994)

15) M. J. Clarke and J. B. Gaul, "Chemistry Relevant to the Biological Effects of Nitric Oxide and Matallonitrosyls", in "Structure and Bonding" vol. **81**, 147 (1993)

16) Th. Woike, W. Krasser, P. S. Bechthold and S. Haussühl, Phys. Rev. Letters **53**, 1767 (1984)

17) J. Tritt-Goc, N. Pislewski and S. K. Hoffmann, Chem. Phys. Letters **268**, 471 (1997) and references therein

18) Th. Woike, M. Imlau, S. Haussühl, R. A. Rupp and R. Schieder, Phys. Rev. B **58**, 8411 (1998)

19) M. B. D. Bloom, J. B. Raynor and M. C. R. Symons, J. Chem. Soc. A (**1971**) 3843; D.

A. C. McNeil, J. B. Raynor and M. C. R. Symons, J. Chem. Soc. A (**1965**) 410

20) J. D. W. van Voorst and P. Hemmerich, J. Chem. Phys. **45**, 3914 (1966)

21)a) J. Schmidt, H. Kühr, W. L. Dorn and J. Kopf, Inorg. Nucl. Chem. Letters **10**, 55 (1974);

b) C. Glidewell and I. L. Johnson, Inorganica Chimica Acta **132**, 145 (1987)

22) J. B. Raynor and M. C. R. Symons, J. Chem. Soc. A (**1970**) 339; J. B. Raynor, J. Inorg. Nucl. Chem. **33**, 735 (1971) and references therein

23) M. C. R. Symons, D. X. West and J. G. Wilkinson, Inorganic Chemistry **15**, 1022 (1976)

24) J. Danon, R. P. A. Muniz and H. Panepucci, J. Chem. Phys. **41**, 3651 (1964)

25) M. C. R. Symons, J. G. Wilkinson and D. X. West, J. Chem. Soc. Dalton Trans. (**1982**), 2041

26) D. E Ellis and G. S. Painter, Phys. Rev. B **2**, 2887 (1970); D. E. Ellis, Int. J. Quant. Chem. **2S**, 35 (1968)

27) D. E. Ellis and D. Guenzburger, "The Discrete Variational Method in Density Functional Theory and its Applications to Large Molecules and Solid-State Systems", in "Advances in Quantum Chemistry" vol. **34**, 51 (1999), and references therein

28) see, for example, R. G. Parr and W. Yang, "Density Functional Theory of Atoms and Molecules", Oxford University Press, New York (1989)

29) S. H. Vosko, L. Wilk and M. Nusair, Can. J. Phys. **58**, 1200 (1980)

30) A. H. Stroud, "Approximate Calculation of Multiple Integrals", Prentice Hall, Englewwod Cliffs (1971)

31) R. S. Mulliken, J. Chem. Phys. **23**, 1833 (1955); **23**, 1841 (1955); C. Umrigar and D. E. Ellis, Phys. Rev. B **21**, 852 (1980)

32) B. Delley and D. E. Ellis, J. Chem. Phys. **76**, 1949 (1982)

33) B. Delley, D. E. Ellis, A. J. Freeman, E. J. Baerends and D. Post, Phys. Rev. B **27**, 2132 (1983)

34) A. Becke, Phys. Rev. A **38**, 3098 (1988)

35) J. P. Perdew, Phys. Rev. B **33**, 8822 (1986); **34**, 7406 (1986)

36) D. M. P. Mingos, Inorg. Chem. **12**, 1209 (1973)

37) J. H. Enemark and R. D. Feltham, "Principles of Structure, Bonding and Reactivity for Metal Nitrosyl Complexes", in Coordin. Chem. Revs. **13**, 339 (1974)

38) S. R. Nogueira and D. Guenzburger, Int. J. Quant. Chem. **54**, 381 (1995)

39) N. V. Vugman, personal communication

40) N. N. Greenwood and T. C. Gibb, "Mössbauer Spectroscopy", Chapman and Hall, London (1971)

41) Z. Zeng, D. Guenzburger and D. E. Ellis, Phys. Rev. B **59**, 6927 (1999)

42) P. Dufek, P. Blaha and K. Schwarz, Phys. Rev. Letters **75**, 3545 (1995)

43) S. Joss, K. M. Hasselbach, H.-B. Bürgi, R. Wordel, F. E. Wagner and A. Ludi, Inorg. Chem. **28**, 1815 (1989)

44) P. Gütlich, R. Link and A. Trautwein, "Mössbauer Spectroscopy and Transition Metal Chemistry", Springer-Verlag, Berlin (1978)

45) A. Abragam and M. H. L. Pryce, Proc. R. Soc. A **205**, 135 (1951)

46) A. Abragam, "The Principles of Nuclear Magnetism", Oxford University Press, Oxford (1961)

47) L. Fan and T. Ziegler, J. Chem. Phys. **94**, 6057 (1991)

48) L. A. Eriksson, O. L. Malkina, V. G. Malkin and D. Salahub, J. Chem. Phys. **100**, 5066 (1994)